



Floodplain chronology and sedimentation rates for the past 200 years derived from trace element gradients, organic compounds, and numerical modeling

Michael Buchty-Lemke¹ · Lukas Hagemann² · Anna-Lisa Maaß³ · Holger Schüttrumpf³ · Jan Schwarzbauer² · Frank Lehmkühl¹

Received: 28 September 2018 / Accepted: 8 July 2019 / Published online: 19 July 2019
© Springer-Verlag GmbH Germany, part of Springer Nature 2019

Abstract

This study evaluates the applicability of trace element and organic contaminant data from a floodplain cross-section as the basis for a numerical model of spatial floodplain dynamics. Using threshold values of pollution-sensitive trace elements and market introduction dates of organic xenobiotics, the sampled sediment is assigned to historical phases to develop a sediment chronology. The investigation is based on a 60-m wide core transect from which sediment samples were analyzed to determine grain-size distribution, trace element inventory, and organic xenobiotic content. In addition, floodplain inundation, flow velocities, and the amount of sediment deposited were numerically modeled using Delft3D to verify the analyses results; conversely, the results of the sedimentary analysis served the input data for the model. Changes in floodplain morphology were interpreted on the basis of a digital elevation model (1 m resolution), historical maps from 1865 AD, and field surveys. The architecture of the alluvial sediments was examined in the cores accounting recent floodplain relief and possible historical factors. The results show a broad range of heavy metal pollutants and the presence of 57 volatile organic compounds in a pattern that reflects multiple deposition processes and phases. Based on these results and the model verification, the sediments were assigned to pre-industrial, industrial, and post-industrial phases, and sedimentation rates of 0.6–1.3 cm a⁻¹ were estimated. The results of this study contribute to a better understanding of the development of small meandering gravel-bed rivers with large floodplains, where suspended sediments predominate.

Keywords Fluvial morphodynamics · Floodplain deposits · Heavy metals · Interdisciplinary approach · Organic pollutants · Pollution history

Electronic supplementary material The online version of this article (<https://doi.org/10.1007/s12665-019-8428-4>) contains supplementary material, which is available to authorized users.

✉ Michael Buchty-Lemke
buchty@geo.rwth-aachen.de

¹ Department of Geography, RWTH Aachen University, Templergraben 55, 52056 Aachen, Germany

² Institute of Geology and Geochemistry of Petroleum and Coal, RWTH Aachen University, Lochnerstraße 4-20, 52056 Aachen, Germany

³ Institute of Hydraulic Engineering and Water Resources Management, RWTH Aachen University, Mies-van-der-Rohe-Straße 17, 52056 Aachen, Germany

Introduction

Floodplain sediments record anthropogenic activities that are coupled with the emission of lipophilic organic and inorganic compounds and thus serve as an archive for cultural and industrial history (De Vos et al. 1996; Demetriadis et al. 2006; Hoffmann et al. 2010; Schmidt-Wygasch 2011; Adánez Sanjuán et al. 2014; Dhivert et al. 2015; Ciszewski and Grygar 2016). In general, such emissions are distributed by rivers as particle-bound compounds and compounds in solution (Owens et al. 2005; Perry and Taylor 2009). Accordingly, floodplain sediments are temporary sinks for these compounds which, when remobilized, bear the fingerprint of human activity within the river basin and beyond (i.e., when originating from neighboring catchments and atmospheric deposition). However, if particle-associated compounds are transported by water, dispersion is variable

because the process of accretion varies. During accretion processes, such as vertical overbank accretion, lateral point bar accretion, or crevasse splay, particle-bound compounds are distributed unevenly via the process-related sorting of grain sizes (Middelkoop 2000; Hürkamp et al. 2009a; Nichols 2009; Ciszewski and Grygar 2016). These processes—and other anthropogenic influences affecting flow dynamics including embankment construction (Ciszewski and Grygar 2016) and subsidence caused by deep coal mining (Bell et al. 2000)—ultimately result in microscale cross-facies variability of the dispersed compounds, both in the vertical and in horizontal profiles.

Lipophilic organic contaminants such as dichlorodiphenyltrichloroethane and its metabolites (DDX) and linear alkylbenzenes (LAB), and anthropogenically elevated potentially toxic trace elements (PTEs), such as Cu, Zn, and Pb, are adsorbed by fine-grained sediments (Gevao et al. 2000; Schulze and Ricking 2005). Hence, fine-grained sediments are a key factor in the distribution of contaminants by floods (Phillips et al. 2000; Malmon et al. 2002; Walling et al. 2003; Förstner 2004; Owens et al. 2005). Changes in sediment load, sedimentation rates, and aggradational and degradational processes induced by human activities directly influence the dispersion of contaminants (Frings et al. 2014), and this is of particular relevance in old industrial regions (Germershausen 2013). Small catchments are thereby more suitable for investigating the distinct signals of anthropogenic activity, as supra-regional signals are superimposed onto local signals in larger catchments. Here, the term ‘small catchments’ refers to those river systems that do not exceed Strahler stream order 3. In general, PTE pollution is ubiquitous in Central Europe, as the population density and the number of industrial facilities are high.

The combination of field measurement and numerical modeling has been successfully undertaken in floodplain research. For example, Pu and Lim (2014) modeled the long-term effects of scouring processes around abutments and compared their results with field measurements. Rahbani (2015) compared the profiles of suspended sediment concentrations from a model with those from the field. Nicholas and Walling (1998) presented a study of overbank processes, combining field-work and a numerical modeling approach to predict realistic patterns of overbank deposition. Their study referred to the models of James (1985) and Pizzuto (1987), which predict suspended sediment concentrations, sediment deposition rates, and deposit grain-size distributions across channel and floodplain cross-sections.

Importantly, local topography influences the rates and patterns of sedimentation in floodplains (Nicholas and Walling 1997), which can be investigated by field-based measurements. However, numerical models are able to predict flow depths and (depth-averaged) flow velocities, which are difficult to measure directly during flood events (Nicholas

and Walling 1998). This underlines the value of adopting a combined approach that employs both field measurement and numerical modeling.

In recent decades, numerous studies have been published that combine multiple methods and which aim to better understand floodplain formation and contamination. Swennen et al. (1994), Gocht et al. (2001) and Witter et al. (2004) combined sedimentological investigations with elemental and/or organic geochemical analysis. Leenaers (1989) supported his sedimentological analyses results with ^{137}Cs dating. With a focus on elemental analysis and GIS approaches (Novakova et al. 2013; Elznicová et al. 2019; Grygar et al. 2016; Fikarová et al. 2018; Famera et al. 2018) combined organic geochemical analysis, chemostratigraphy, dating, and electric resistivity tomography (ERT). With an emphasis on dating, the investigations by Heim et al. (2004, 2005, 2006) were also based on a combination of organic geochemical analysis and chemostratigraphy.

However, most of these studies have focused on large streams. Normally, such systems are embedded in a confined channel that prevents the floodplains from being affected by degradation processes in the river corridor. As a result, there is a general lack of knowledge about the floodplains of smaller streams under near-natural conditions.

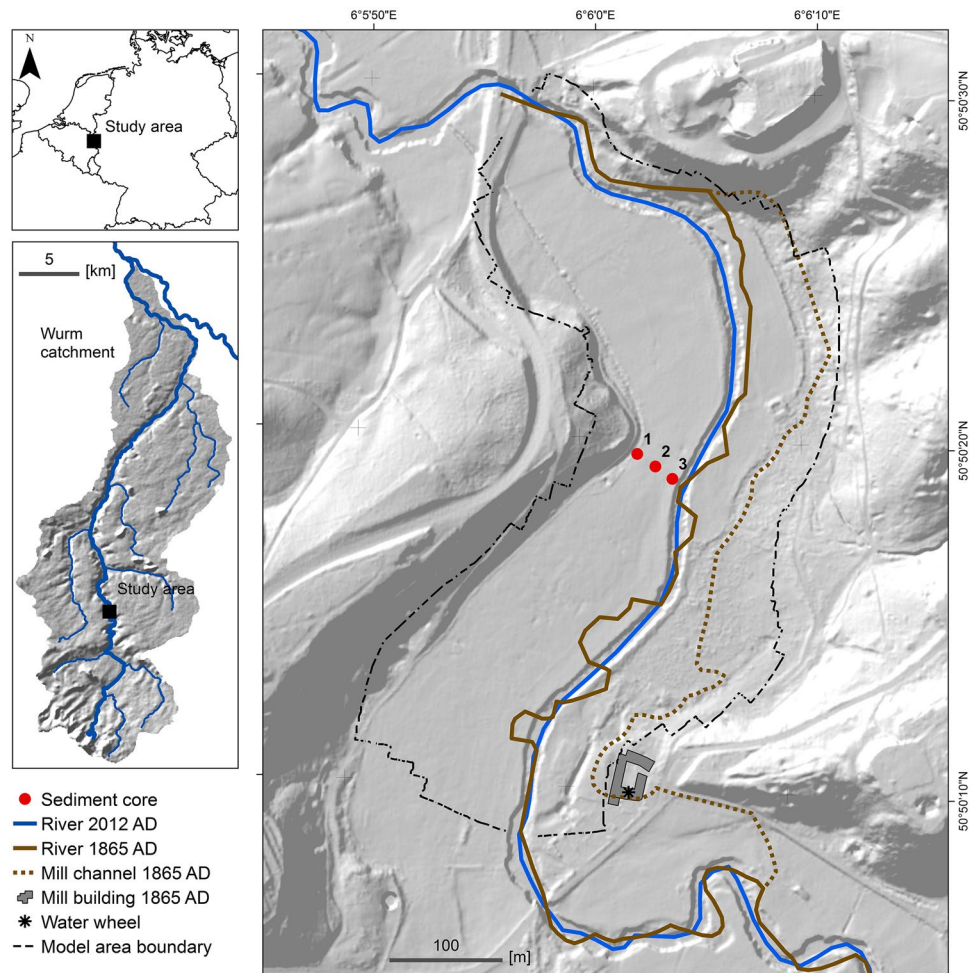
The aim of this research is to investigate the sedimentation rates of floodplains over a 1-km long reach of the Wurm River in the Lower Rhine Embayment, Germany, by focusing on the novel and interdisciplinary combination of geomorphological and geochemical dating data as the input for numerical modeling. The Wurm River has been—and continues to be—influenced by various anthropogenic factors including water mills, underground coal mining, and urbanization, all of which have recently been studied by Buchty-Lemke (2018), Buchty-Lemke and Lehmkuhl (2018), Hagemann et al. (2018) and Maaß and Schüttrumpf (2018, 2019). The results from the different methods are combined to develop a comprehensive synthesis, which both improves the reliability of the individual results and creates a more holistic understanding of the diversity of contamination in floodplains.

Materials and methods

Study area

The investigation was based on a 1-km long segment of the Wurm River, which is a low-order stream (catchment area = 350 km², length = 56 km, Strahler stream order = 3) in the west of Germany at the border with the Netherlands (Fig. 1). The Wurm River is representative of rivers that are, on the one hand, strongly affected by anthropogenic activities, and on the other hand, are in near-natural condition. In

Fig. 1 Study area showing the location of the core transect and the model area boundary. The historic river course, mill channel, and mill building are mapped from a cadastral map (see Online Resource 1) from 1865 AD. Map base: hillshade derived from a LiDAR DEM (Land 2017)



the headwaters, the city of Aachen represents a broad spectrum of industrial pollution sources from industrialization as well as being the source of a significant amount of municipal wastewater. These forms of pollution have increased considerably with population growth from 170,000 in 1950 AD to 240,000 in 1980 AD (Eschweiler and van Eyll 2000). The upper river course emerges from the Eifel foothills with an altitude of approximately 250 m above sea level (a.s.l.) into a Pleistocene rolling-hill landscape. Due to a complex tectonic setting, Carboniferous layers strike out in the walls of the valley. This is the basis for a coal mining history dating back to the early Middle Ages and which creates the preconditions for potential mining subsidence, which can occur as the result of collapsing bedrock above industrial-scale coal extraction cavities (Heitfeld et al. 2005). The beginning of industrial coal mining in the middle of the nineteenth century, with a peak in the early twentieth century, was followed by a rapid decline in the late twentieth century (Eschweiler and van Eyll 2000). Historic pollution sources were distributed all over the city of Aachen in the headwater area. For example, the steel mill Aachener Hütten-Aktien-Verein Rothe Erde, which was established in 1847 (Bruckner 1967),

was one of the world's largest steel factories in c. 1890 and was closed in 1926. The applied basic Bessemer process led to a substantial amount (approximately 2,000,000 m³) of basic slag being produced, containing FeO₂, MnO₂, SiO₂, and tricalcium phosphate, that was stored in storage sites (Hasse 2000) and sold as fertilizer (Käding 2005).

Today, two wastewater treatment plants (WWTP) with a total capacity for a population of 550,000, apply tertiary treatment and discharge reclaimed water into the Wurm River. Before the upgrade of the WWTPs in the 1980s, approximately 70% of the Wurm River's streamflow was untreated wastewater. This scale of this pollution manifested itself in the form of odorous black water with floating foam (Fischer 2000). Table 1 gives an overview of the historical emissions in the wider study area with a focus on the headwater and upper course of the Wurm River.

The perennial, pluvial flow regime creates a mean flood discharge of approximately 25 m³ s⁻¹ and a mean discharge of approximately 2 m³ s⁻¹ in the upper river course, of which up to 90% (Weber 1991; Hoppmann 2006) consists of treated wastewater from the main WWTP of the city of Aachen (with a mean discharge of 0.85 m³ s⁻¹ in 2015). The

Table 1 Chronology of emissions within the catchment of Wurm River

Century	Substances	Sources	References
Nineteenth century	Dyes and soaps	Textile craft	Dahmen (1925)
Early middle ages	Polycyclic aromatic hydrocarbons and sulfate	Coal mining	Malz (1972)
Eighteenth century	Heavy metals, polycyclic aromatic hydrocarbons, and cyanide	Steel mills, dyeing plants, gas plant, and glassworks	Meyer (1908), Bruckner (1967) and ABANDA (2013)
Nineteenth century	Heavy metals, polycyclic aromatic hydrocarbons, and cyanide	Coking	Stelzer (2000)
Twentieth century	Heavy metals, barium sulfate, and a spectrum of organic substances in domestic use	Coal mining, glassworks, and municipal wastewater	Stelzer (2000) and Fischer (2000)

drainage area above the study site is approximately 90 km²; the valley narrows from south to north from approximately 250–100 m (see Buchty-Lemke 2018). The difference in altitude between the floodplain and the surrounding plateau is approximately 50 m. The width of the river varies between 10 and 15 m with a general slope of 1.9‰.

The river is incised approximately 2 m into the floodplain, creating steep banks of fine-grained alluvial sediment that are subject to lateral erosion. The incision of the riverbed is the result of the abandonment of a water mill at the head of the study segment (see Fig. 1) (Buchty-Lemke and Lehmkuhl 2018). This historic water mill (Alte Mühle) divided the river into a main channel and a parallel mill channel. The mill was built in the Early Middle Ages (c. 867 AD), and was abandoned c. 1900 AD. It was used for flour and oil production (Vogt 1998) and, therefore, was not a potential source of contaminants. Today, the mill channel is separated from the river but persists as a swampy drainage channel.

The main phases of land-use change in the study area were elaborated by Nilson (2006). In summary, the main changes involved the transition from agriculture to pasture and reforestation in the nineteenth century, and successive urbanization since the mid-twentieth century (Buchty-Lemke 2018). A mine-water inlet of the ‘Gouley’ coal mine (with a first historic reference dating to 1599 AD and being abandoned in 1969 AD; Wrede and Zeller 1988) is located approximately 400 m upstream of the study segment. Details of the geological setting are provided by Hindel et al. (1996).

GIS, grain-size analysis, and elemental analysis

The geomorphological context, soil properties, sedimentological characteristics, and riverscape development were investigated by means of field-work, examination of historical maps from 1865 AD, aerial photographs from 1974 AD and later (Bezirksregierung Köln 2017), and a

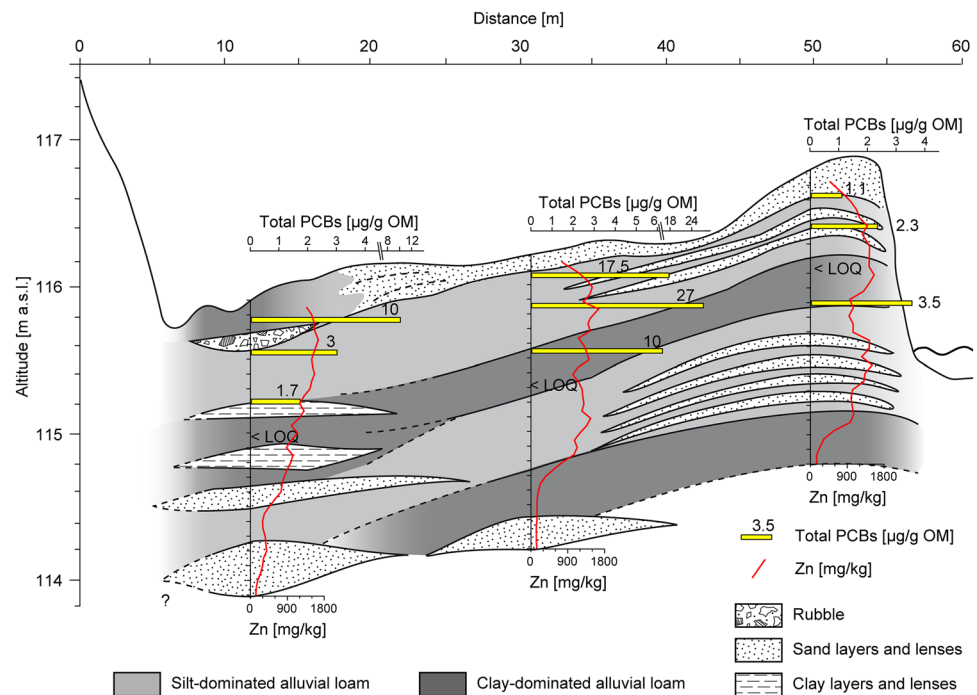
LiDAR-derived DEM¹ (spatial resolution = 1 m, height resolution ± 0.2 m) (Land 2017) with GIS (see Online Resource 1). The inventory and distribution of contaminants, and the sedimentological properties of the floodplain sediments were analyzed on the basis of a core transect with three cores (spacing = 20 m, depth = 2 m in each case, sampling interval = 5 cm). Core drilling was undertaken with a gas-operated handheld jack-hammer with lined steel corers (1 m in length, 5 cm in diameter, and compaction of < 5%). The liners were opened with a customized saw, which enabled the plastic liners to be cut laterally without cutting the sediment filling. The selection of the sampling areas was based on preliminary work that identified the floodplain as being potentially affected by mining subsidence (see Online Resource 1). In addition, the transect was selected as being representative of the general character of the floodplain. For grain-size analysis and CHNS determination of the total carbon content (TC), the sediment samples were dried, homogenized, and sieved to obtain the fine fraction (< 2 mm). The concentrations of trace elements were measured in the < 63 µm fractions via X-ray fluorescence. Details on sample preparation and measurement are provided by Schulte et al. (2016).

Organic geochemical analyses

Organic geochemical analyses were carried out for four bulk samples of each core (15–25 cm, 35–45 cm, 65–75 cm, and 85–95 cm depth) using a sequential solid–liquid extraction following Berger et al. (2016). First, extraction was performed on 20 g of field-moist and untreated sediment from each sample using ultrasonication and stirring with acetone and *n*-hexane as the solvents. After volume reduction and drying with anhydrous granulated sodium sulfate, elemental sulfur was removed by the addition of activated copper powder. The column chromatographic fractionation was

¹ Digital elevation model (DEM) generated by the surveying method ‘Light Detection and Ranging’ (LiDAR).

Fig. 2 Stratigraphy of the core transect (see Online Resource 2 for photographic documentation of the cores) with example concentrations of elements (Zn) and organic compounds (PCBs)



conducted using *n*-pentane, dichloromethane (DCM), and methanol at different ratios following Schwarzbauer et al. (2000). 50 µL of a surrogate standard (6.28 ng µL⁻¹ of deuterated benzophenone, 5.83 ng µL⁻¹ of fluoroacetophenone, and 6.03 ng µL⁻¹ of deuterated hexadecane) were added to each fraction after the polar fractions were methylated by the addition of a methanolic diazomethane solution. Prior to analysis, the sample volume was reduced to 50 µL using a rotary evaporator at room temperature.

After measurement using gas chromatography–mass spectrometry (GC–MS), a non-target screening was been carried out to ensure a comprehensive overview of any present volatile organic compounds within the analyzed samples. Organic matter (OM) content was determined by loss on ignition (LOI) measurements at 550 °C for 4 h according to Stock et al. (2016).

Numerical modeling

The effects of the deposition of fine sediment during overbank flood events were numerically modeled using Delft3D-FLOW software in 2D (depth-averaged) mode (Deltares 2016). This floodplain model has already been successfully applied to study the long-term effects of mining-induced subsidence on the sediment trapping efficiency of floodplains (Maaß and Schüttrumpf 2018). The model was based on the physiographic characteristics of the 1-km long segment of the Wurm River. The total number of cells was equal to 18,383 grid cells including 1513 grid cells for the main channel with an average cell size of 8.33 m². The topography

of the floodplain was derived from the LiDAR DEM. The existing bathymetry of the river channel was derived from cross-sectional profiles. The model was laterally restricted by the hillsides of the valley. The calibration of the numerical model was directly linked to the results of the trace element and organic geochemical analyses as discussed in Sect. "Results and implications". The boundary conditions correspond to those recently published by Maaß and Schüttrumpf (2018). Specifically, a quasi-steady time-dependent inflow hydrograph was applied at the upstream boundary and a discharge and water-depth relationship was applied at the downstream boundary.

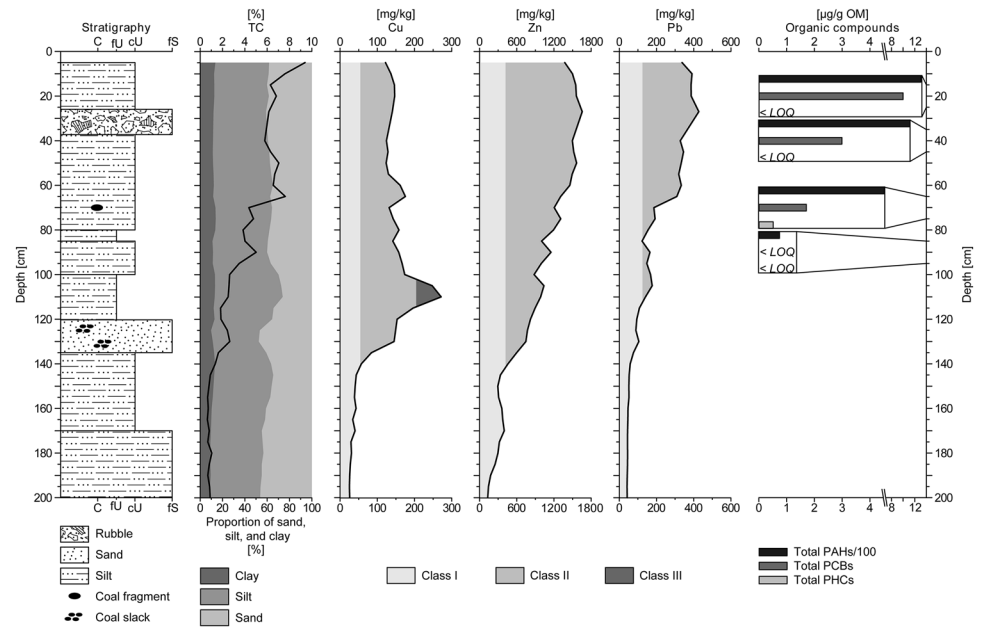
Results and implications

Soils, sedimentology, and geomorphological context

Sediment cores 1, 2, and 3 were correlated in a transect from the wall of the valley towards the river (Figs. 1, 2). The floodplain is currently used for extensive grazing. All of the cores were categorized as Fluvisols.² Their general appearance was characteristic of overbank lithofacies, with a dominance of silt and a massive sediment structure with

² Horizon codes according to the World Soil Classification of the Food and Agriculture Organization of the United Nations (FAO) are used for the soil description.

Fig. 3 Core 1: stratigraphy, grain size, TC content, and analysis of trace elements and organic compounds. Background content for trace elements are indicated by classification I to III (see Table 2). Bulk samples for organic geochemistry were taken at depths of 15–25 cm, 35–45 cm, 65–75 cm, and 85–95 cm



rare fine laminations and thin lenses of fine sand (Online Resource 2). The lower third of the cores were from below the groundwater table. Fine fragments of coal and thin layers of fine sand were present in the subsoil. Normal and reverse grading sequences were somewhat indicated at the base and at the top of the sediment cores. There was a tendency for horizontal coarsening of the topsoil, moving towards the river. As shown in Fig. 2, the central part of the alluvium was characterized by a dominance of alluvial loam. Coarser grain sizes were present at the top and at the base of core 2. Core 1 and core 3 were structured by lenses and layers of fine sand with interbedded alluvial loams, with abundant silt and clay.

Core 1 (Fig. 3) at the wall of the valley was characterized by a bog-like topsoil with a TC content of 7–9% (CHNS analysis) above allochthonous anthropogenic sediment that covered a buried humic topsoil. From 50 to 95 cm depth, a Bg horizon was identified. The Bg was underlain by a Cr horizon with an interbedded Cg layer between 130 and 145 cm depth. The texture was dominated by grain sizes of 20–40 μm (D_{50}) with two sharply delimited peaks of 140 μm (mode). The upper peak represents rubble filling (e.g., construction waste and other unknown anthropogenic materials) and the lower peak represents alluvial sediment with a slight coarsening in the upward direction. Clay content was generally high at 8–13% throughout the core. Coal fragments (0.5 \times 1 cm) from the former underground coal mining industry in Aachen were found at a depth of 70 cm, and small amounts of coal slack were present at a depth of 120–130 cm.

Core 2 (Fig. 4) had a thin layer of alluvial fine sand, covering an Ah horizon with a seamless transition to the

underlying B horizon. Small sand lenses at 80 cm depth separated the B from a Br/Cr horizon. The massive subsoil below 80 cm was subject to gleying and reduction, with mottling of iron, where the pore volume was higher at the core base. The dominating grain sizes were similar to core 1, with the peak in the topsoil (mode = 127 μm) representing fine-sand overbank deposits. The clay content varied between 8 and 16%; the highest proportions of clay were observed at 70 cm and 140 cm depth. A coal fragment (0.2 \times 0.5 cm) was found in a depth of 150 cm, and coal slack was sparsely detected at 150 cm and 170 cm, but was abundant at 190 cm depth.

The topsoil of core 3 (Fig. 5) extracted from the natural levee was characterized by laminated fine-sand overbank deposits. The B horizon expanded from 10 to 80 cm depths and was underlain by a Cr layer (80–200 cm) with interbedded Cg deposits at 130–155 cm depths. Fine brick fragments were found between 55 and 60 cm depths. The alluvial loam in the subsoil was interspersed with coal slack below 50 cm depth; coal fragments (0.1 \times 0.5 cm) were found at a depth of approximately 140 cm. Several fine sand peaks (mode = 140–150 μm) and a medium-to-coarse sand lens (115–120 cm) were also identified. A slight upward fining was observed between 130 cm and 150 cm depths. In general, the D_{50} grain size of core 3 was more heterogeneous than in core 1 and core 2; medium silt was abundant across core 3 and clay content exceeded 12%.

The width between the western and eastern valley confinement is 240 m. Generally, floodplain width provides information on the long-term importance of geomorphic processes. Narrow floodplains provide an indication of important incision phases and vertical erosion, whereas

Fig. 4 Core 2: Stratigraphy, grain size, TC content, and analysis of trace elements and organic compounds. Background contents for trace elements are indicated by classification I to III (see Table 2). Bulk samples for organic geochemistry were taken at depths of 15–25 cm, 35–45 cm, 65–75 cm, and 85–95 cm

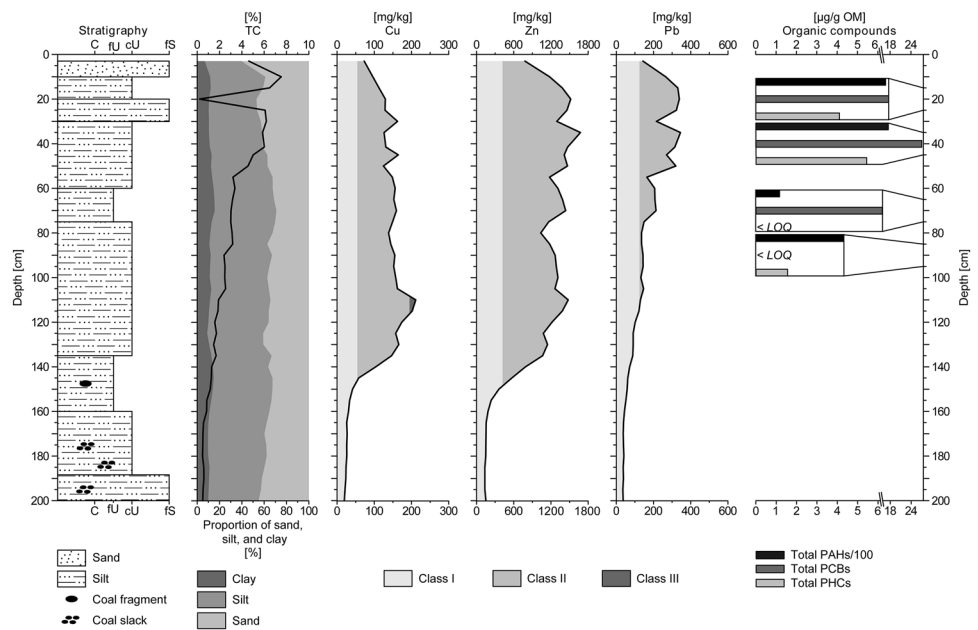
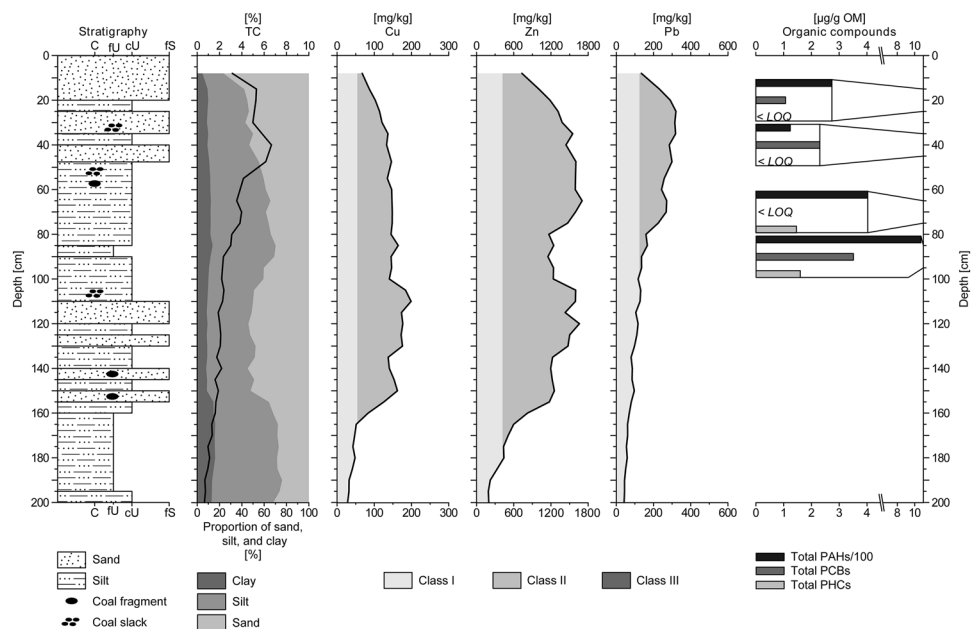


Fig. 5 Core 3: Stratigraphy, grain size, TC content, and analysis of trace elements and organic compounds. Background contents for trace elements are indicated by classification I–III (see Table 2). Bulk samples for organic geochemistry were taken at depths of 15–25 cm, 35–45 cm, 65–75 cm, and 85–95 cm



wide floodplains suggest lateral erosion (Notebaert and Piégay 2013). At the Wurm River site, these historical landscape development processes might be of secondary importance given that the floodplain width is restricted by the valley slopes. Historical maps (Online Resource 1) show a meander bend towards the west with the outer bank approximately at the thalweg of the modern channel (Fig. 1). The channel was partly straightened in the 1930s (according to local knowledge) and the floodplain is characterized by a dominance of overbank vertical-accretion

deposits. Although the Wurm River is noted as a gravel-bed river (Landesumweltamt Nordrhein-Westfalen 2005), the lack of coarse sediment caused by the abundance of impervious areas in the headwaters gives rise to the dominance of cohesive sediment. As fine-grained sediments are subject to compaction when the proportion of organic matter is high (Törnqvist and Bridge 2002), and because inundation frequency is lowered due to channel incision, the floodplain surface is tilted approximately 1.3° and slopes towards the western wall of the valley.

Table 2 Local empirical threshold values of selected trace elements based on the frequency distribution of the elemental analysis data set

	Class I	Class II	Class III	TEC	PEC	Background
Cu (mg kg ⁻¹)	< 55	55–205	> 205	31.6	149	17.3
Zn (mg kg ⁻¹)	< 420	420–1740	> 1740	121.0	459	68.1
Pb (mg kg ⁻¹)	< 125	125–455	> 455	35.8	128	32.0

Sediment quality guideline values (threshold effect concentration (TEC) and probable effect concentration (PEC) after MacDonald et al. 2000) and mean background content for Europe (Kabata-Pendias 2011) are given for comparison

Trace element content and distribution

Depending on the industrial and cultural history within a river basin, the inventory of polluting compounds is heterogeneous. To illustrate the concentration gradient caused by anthropogenic activities, the pollution-sensitive trace elements Cu, Zn, and Pb (Swennen and Van der Sluys 2002) were determined as representative pollutants for the Wurm River basin, as these are present in the emissions of the following activities in the headwaters: coal mining and processing, metal production and processing, textile manufacturing, tire and glass production, sewage sludge and liquid manure spreading, and municipal wastewater treatment.

To structure the vertical trace element gradient, the content levels were categorized into three pollution classes: (I) pre-industrial and pristine sediment (e.g., natural background); (II) moderately polluted sediment caused by non-point consumer-related or industrial sources or a mix of strongly polluted and pristine sediment created by remobilization; and (III) strongly polluted sediments resulting from industrial point sources or waste disposal sites. Following the approach of Buchty-Lemke (2018), this classification was based on empirical local threshold values (Table 2) derived from the analysis of the transect samples (see Online Resource 3).

The trace element proportions of core 1 show a generally increasing trend from bottom to top, with the lowest values at the core base, elevated values in the subsoil and topsoil, and a decrease in the modern topmost sediments (Fig. 3). In the lower subsoil, sediments corresponded to class I. At approximately 140 cm (Zn and Cu) and 120 cm (Pb), there was an inflection point in the depth gradient where the concentrations of these elements rose from class I to class II. Moving upwards, the PTS concentrations remained at class II levels; Cu concentrations ranged between approximately 120–170 mg kg⁻¹ with a peak exceeding the threshold of class III at a depth of 100–115 cm. Zn values increased progressively from 131 mg kg⁻¹ at the base of the core to 1700 mg kg⁻¹ in the topsoil; the topmost sediments were characterized by Zn concentrations that decreased in the upward direction to 1300 mg kg⁻¹. Pb concentrations fluctuated at around 330 mg kg⁻¹ in the topsoil in the depth range 0–65 cm. Below this, the concentrations were close to

the class I/class II threshold. The lowest values occurred in the lower subsoil, ranging from 44 to 100 mg kg⁻¹.

Core 2 showed similar characteristics with respect to trace element patterns with the exception of Cu, which only slightly exceeded the class II/class III threshold at a depth of 110 cm (Fig. 4). The Cu peak was similar to core 1, but was less pronounced. The Zn gradient did not progressively decrease from the surface as in core 1, but was more similar to the Cu pattern, showing a rather constant concentration within the range 1100–1600 mg kg⁻¹. Core 2 was characterized by a PTE decrease in the topsoil that was more distinct than in core 1. In the case of Cu and Zn, the inflection points in the depth gradients were shifted downwards by approximately 10 cm, while the Pb inflection point was shifted upwards by approximately 40 cm.

Core 3 was characterized by a PTE pattern that was similar to core 1 and core 2, but with the following exceptions: the class I to class II inflection points for Cu and Zn were the lowest within the transect, occurring at a depth of 165 cm and 175 cm, respectively; and the Pb inflection point was similar to core 2 (at a depth of 75 cm) (Fig. 5). As in the other cores, the PTE content of core 3 was lower in the topmost sediments, decreasing by a factor of two. Cu and Pb were at natural background levels, being classified as class I.

The PTE depth gradients indicate that the alluvial sediment within the floodplain has been subject to the input of elevated trace elements caused by anthropogenic activities. The inflection points that mark the transition from class I to class II sediments imply that, below these points, anthropogenic emissions have been absent or too low to exceed the natural background levels. Above the inflection points, the concentrations of PTEs rose significantly—to moderate and high values—corresponding to intense pollution from the industrialization. Accordingly, the inflection points mark the beginning of the industrialization in the study area. For example, Zn arises mainly from industrial activities such as mining and coal combustion (Wessels et al. 1995; Salmiinen et al. 2005). The topmost sediments in all of the cores showed a reduced PTE content, as modern sedimentation is no longer subject to intense pollution due to environmental protection measures. The variability in PTE content across the transect can be explained by variations in grain-size distributions: the higher the proportion of sand, such as in the

natural levee sediment at the top of core 3, the lower the overall PTE content. In general, no effect of TC on PTE concentrations was observed, as shown in core 1 (Fig. 3) where the Cu peak occurred in the same depth range as a decrease in TC content. However, in the same example, it can be seen that the proportion of silty sediment had a significant impact on the distribution of PTEs.

Organic geochemical analyses

The analysis identified 57 volatile organic compounds stemming from both natural and anthropogenic sources. These compounds enter the environment via point sources (e.g., WWTPs) and/or non-point sources (e.g., exhaust fumes and agriculture). Apart from polycyclic aromatic hydrocarbons (PAHs) and polyhalogenated carbazoles (PHCs), all of the identified compounds were anthropogenic pollutants that do not occur naturally. These included chlorinated benzenes, chlorinated anisoles, polychlorinated biphenyls (PCBs), polychlorinated naphthalenes (PCNs), linear alkylbenzenes (LABs), and DDXs (bis(4-chlorophenyl)-2,2,2-trichloroethane (DDT) and its metabolites). With respect to PHCs, it is yet unknown how natural and anthropogenic sources of these pollutants can be best distinguished (Reischl et al. 2005; Grigoriadou and Schwarzbauer 2011; Mumbo et al. 2016).

The total amounts of the compound groups (see Online Resource 4) were highest for PAHs [up to 4200 $\mu\text{g kg}^{-1}$ dry weight (dw)] followed by PCBs [up to 55 $\mu\text{g kg}^{-1}$ dw], and PHCs (up to 11 $\mu\text{g kg}^{-1}$ dw). With the exception of PAHs and PCBs, concentrations of all the other identified compounds were only slightly, if at all, above the limit of quantification (LOQ) (<0.5 to 11 $\mu\text{g kg}^{-1}$ dw). Thus, Figs. 3, 4 and 5 only show the results for PAHs, PCBs, and PHCs. The LOI measurements revealed that OM content ranged from 5.3 to 13.8%. The concentrations of organic compounds, which tend to adsorb to organic matter, were, therefore, normalized to OM for improved comparability.

For core 1 (Fig. 3), concentrations for PCBs and PAHs show a pattern of decreasing concentrations with sampling depth. While PAHs and PHCs were present in all of the four subsamples (20 cm, 40 cm, 70 cm, and 90 cm depths), anthropogenic pollutants were present in the upper three samples but not in the lowest one. Accordingly, it can be assumed that sediment from 90 cm and below was deposited before 1900 AD given that the extensive usage and corresponding emission of synthetic organic compounds begin in the early twentieth century.

In core 2 (Fig. 4), concentrations showed a decreasing trend with sampling depth for most of the substance groups. Therefore, the overall pattern was similar to core 1; anthropogenic pollutants occurred in all four subsamples. Results for core 3 (Fig. 5) showed a slight increase in the concentrations of PAHs, PCBs, and PHCs with depth.

In summary, it can be stated that the concentration profiles for core 1 and core 2 were similar, whereas core 3 depicted a different pattern. Measured concentrations were highest in core 2 followed by core 1 and core 3. The investigated wetland sediments were ubiquitously contaminated by a large number of synthetic organic compounds, although measured concentrations were generally very low. Such low concentrations limit the explanatory power of the observed trends and do not allow any correlation to be made with known periods of emission. The low concentrations may reflect the reworking of polluted and pristine sediments. However, the mere presence of synthetic organic compounds can be used to determine a maximum age for the investigated sediments. Despite the occurrence of elevated pollutant concentrations in the upper subsoil, the patterns of trace elements and organic compounds did not indicate a clear, mutual influence. Even though some pollution sources emit both trace elements and organic compounds, possible relationships were blurred in the mixed geochemical signal.

Numerical modeling results

The numerical model simulations provide retrospective results for the last 200 years and give insights into the long-term development of sediment deposition on the floodplain of the Wurm River. The results and details of the hydrodynamic and morphodynamic calibration are published in Maaß and Schüttrumpf (2018).

With a sediment input of 5 kg m^{-3} for each single modeled discharge of the quasi-steady hydrograph, the sedimentation rates were determined by dividing the total amount of sediment deposited on the floodplains by the modeling time. The average sedimentation amount was 0.5 m on the right floodplain and 0.95 m on the left floodplain.

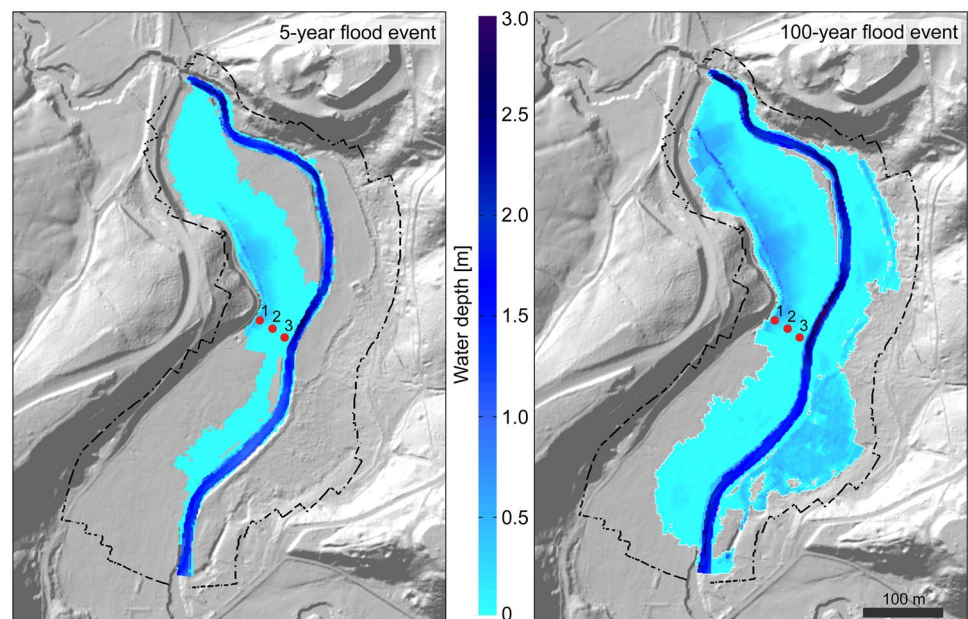
The estimated water depths, flow velocities and cumulative sedimentation depths for the three cores are presented in Table 3. All of these parameters increased with increasing water discharge. Even though the transect was located in a narrow valley reach (confinement ratio 8.8, after Nagel et al. (2014)), the modeled sedimentation rates were quite high in this area (see Fig. 7). This contradicts the conclusions of Notebaert and Piégay (2013), which suggest that a narrow floodplain should be characterized by erosion due to increased flow velocities. The floodplain inundation of the five-year flood results from a backflow entering the floodplain further downstream (see Fig. 6) and causes irregular water depths across the transect. The transect was not flooded entirely, as the bankfull discharge was not exceeded. The modeling indicates that locations of core 1 and core 2 would be inundated to a greater depth than core 3. Accordingly, the cumulative sedimentation depth of core 3 is lower than of core 1 and core 2. In case of a 100-year flood, water depths compensate the relief of the floodplain, rising to a

Table 3 Parameters estimated by numerical modeling of mean water level (MW), mean high water level (MHW), a historical 5-year flood (5-year), and a historical 100-year flood (100-year)

Event	Dis-charge (m s^{-1})	Water depth (cm)			Flow velocity (cm s^{-1})			Cum. sedimentation (cm)					
		Channel	Core		Channel	Core		Channel	Core				
		3	2	1		3	2	1		3	2	1	
MW	2.5	119	0	0	0	33	0	0	0	0	0	0	0
MHW	10	178	0	0	0	85	0	0	0	0	0	0	0
5-Year	20	234	0.5	7	23	104	5	<0.1	<0.1	0	0.3	1.2	1.3
100-Year	40	282	46	110	126	82	81	38	34	0	5	5	5

Cumulative sedimentation values refer to depth accumulation from a single 5-year flood event and a single 100-year flood event, respectively. Values given are grid-cell averages (cell size = 8–22 m^2)

Fig. 6 Modeled inundation for 5-year and 100-year flood events. Symbols are explained in Fig. 1. In the case of a 5-year flood, inundation begins from the downstream left bank at the lower model boundary



uniform water level. In comparison to the location of core 3, core 1 and core 2 would be affected by stagnant water with lower flow velocities compared. Core 3 is located close to the riverbank and, thus, would be directly affected by overflowing water.

Discussion

The measurements of organic and inorganic pollutants allow the estimation of sedimentation rates for the study area. In consideration of the geomorphological interpretation of the floodplain structure, three methodically different estimations were performed. The estimation from trace element data was based on the inflection points in the PTE gradients described in Sect. "Results and implications"; estimation from organic compounds was based on the date of the market introduction of specific synthetic compounds; and the sedimentation rates estimated via numerical modeling were

based on the calculated inundation frequencies. The dating rationale based on the PTE concentrations and their vertical distributions as described in Sect. "Trace element content and distribution", and the contents, vertical distribution, and market introduction date of organic xenobiotics as described in Sect. "Estimation of sedimentation rates via 'chemodating' with organic xenobiotics", are summarized in Table 4. The results are discussed in the following sections based on this rationale.

Estimation of sedimentation rates via trace element gradients

When trace element concentrations are elevated due to anthropogenic activities, the vertical gradients of PTEs can be used as stratigraphic time markers (Hudson-Edwards et al. 1998; Dobler 2000; Birch et al. 2000; Middelkoop 2002; Hürkamp et al. 2009b; Grygar et al. 2012). As shown in Sect. "Results and implications", the PTE gradients

Table 4 Dating rationale developed on basis of inflection points in the vertical distribution of PTEs, their corresponding time spans, and the appearance of organic marker substances and their market introduction date

Trace element/substance group	Corresponding age AD (approximation)	Justification	Local or supra-regional	References
Pollution-sensitive trace elements (Cu, Zn, and Pb)	1830 ± 15	Marker for early industrialization, e.g., the first steam boiler factory in 1814, the first steam engine for coal extraction in 1816, and the construction of the Aachen-Cologne railway in 1841	Local	Curdes (1999) Nilson (2006)
Cu	1870 to 1880	Marker for the intense industrialization, exemplary industry, e.g., needle production	Local	Meyer (1991) von Coels (1991)
Zn	1890–1910	Marker for the so-called Gründerzeit period, in which there was extensive use of zinc-coated (galvanized) construction materials	Local	Buchty-Lemke (2018) Curdes (1999) Umweltbundesamt (2001)
Pb	1970–1980	Marker for traffic, reflecting a growing level of individual motorization	Local	Eschweiler and van Eyll (2000)
PCN	1910 ^a	Marker indicating a maximum age since market introduction and the large scale production of synthetic compounds	Supra-regional	Falandysz (1998)
PCB	1930 ^a		Supra-regional	Shiu and Mackay (1986)
LAB	1960 ^a		Supra-regional	Eganhouse (1986) Zeng and Yu (1996)

The reference date for the calculation of the sedimentation rates was 2014 (the date of sampling)

^aMarket introduction date

identified in the study cores showed distinct inflection points, where the threshold from background levels (class I) to pollution (class II) was exceeded. These inflection points were used to estimate sedimentation rates since industrialization (i.e., a bottom-up increase from class I to class II, or a top-down decrease from class II to class I).

In 1814 AD and 1816 AD, the first steam boiler factory and the first steam engine for coal extraction formed the basis for significant industrial impact in the Aachen region (Curdes 1999), boosted by the construction of the first railway from Aachen to Cologne in 1841 AD (Nilson 2006). Accordingly, the corresponding year for the inflection points that marked the shift from class I to class II was defined as 1830 AD ± 15 years. The resulting sedimentation rates between 1830 ± 15 and 2014 (the year of sampling) are presented in Table 5. As the trace elements could be relocated vertically, these ages represent maximum ages. Hence, the derived sedimentation rates were biased in terms of a possible overestimation.

An approximate verification of this estimation can be achieved by matching historical developments in the wider study area with the sedimentation values converted to years. For example, when converting the sedimentation rates of core 1, the Cu peak at a depth of 105–110 cm corresponds to approximately 1870–1880 AD, which was when intense

industrialization began in Germany. During this time, for example, Cu from the neighboring Inde River catchment was processed in the study area in needle factories (Meyer 1991; von Coels 1991). Another example is the increase in Zn concentrations to more than 1000 mg kg⁻¹, which was identified at a depth of approximately 90–100 cm. This correlates with the zenith of the so-called ‘Gründerzeit’ period (1890–1910 AD), a construction boom during which many new districts were developed and many Zn-containing materials were used. When Zn-containing construction parts such as galvanized gutters, rooftops, or waterspouts corrode, Zn compounds can enter the environment (Umweltbundesamt 2001). Comparable trace element concentrations were documented by Middelkoop (2002) for the Rhine River for the period after 1860 AD. Furthermore, with the growing level of individual motorization and the improvement in road traffic infrastructure in the 1970s (Eschweiler and van Eyll 2000), Pb emissions rose. Accordingly, the vertical gradient of Pb in the sample cores further supports the estimates of sedimentation rates, as the highest content in core 1 and core 3 corresponded to the period 1970–1980 AD.

Modern PTE sources include rain wash from trafficked areas (i.e., wear of tires and breaks) or industrial areas, exhaust fumes from traffic, and the corrosion of galvanized

Table 5 Estimation of mean sedimentation rates based on the applied approaches

Core	Approach			Mean annual sedimentation rate			
	(1) Depth of the first elevated content (inflection points) of Cu and Zn (cm)			Trace element-based sedimentation rates (cm a ⁻¹)			
1	140			0.75			
2	145			0.8			
3	160 (Cu)/180 (Zn)			0.85/0.95			
	(2) Depth of the first occurrence of a synthetic compound (cm)			Organic compound-based sedimentation rates (cm a ⁻¹)			
	PCN	PCB	LAB	90–85 cm	85–65 cm	65–35 cm	35–0 cm
1	65	85 ^a	65 ^a	–	0.7	1.3	
2	65	85	90 ^a	1.8			
3	90	90	90 ^a	1.8			
	(3) Modeled inundation frequency and sediment load			Numerical modeling-based sedimentation rates (cm a ⁻¹)			
1	Inundation begins at a 5-year flood			0.8			
2	Sediment load at the upper model boundary = 5 kg m ⁻³ per discharge class			0.8			
3				0.6			

^aYoungest identified compound in the corresponding sample as used for calculation of sedimentation rates

safety barriers (de Miguel et al. 1997; Monaci and Bargagli 1997; Legret and Pagotto 1999; Umweltbundesamt 2001; Hillenbrand et al. 2005; MKULNV NRW 2009; Callender 2014). Aside from any grain size effects, the activation of such sources could explain why the measured Zn concentrations did not decrease to the natural background levels in the topmost sediments as observed for Cu and Pb in core 2 and core 3. A decrease to natural background levels would be expected as a consequence of measures to reduce environmental pollution since the 1970s (Paul 1994), which have documented by various studies in Western Europe (Bábek et al. 2011; Martin 2015 and references therein). The reduction of the levels of Pb in the topsoils of the sampling sites might relate to the “gradual shift from leaded to unleaded petrol” (de Miguel et al. 1997, p. 2733), which dates to 1971–1974 AD in Germany (Wessels et al. 1995). Similar distribution patterns of Pb were reported by Heim et al. (2004) for the Lippe River in North Rhine-Westphalia, Germany. As atmospheric fallout can be a significant source for PTEs (Nicholson et al. 2003), the prevailing west-southwest winds in this region (Havlik 2001) might have contributed to the PTE inventory by transferring pollutants from Wallonia (Belgium)—an important location for heavy industry in the early and peak industrial era. Such emissions might be the cause of unidentifiable contamination that was present in the subsoil samples and which did not present a clear pattern that corresponded to historical events.

Estimation of sedimentation rates via ‘chemodating’ with organic xenobiotics

Synthetic compounds and compound groups including Methyl-triclosan, DDX, PCNs, PCBs, and LABs do not occur naturally and can, therefore, be assigned to a specific market introduction date. In theory, the occurrence of such substances provides information about the age of the sediment (Gocht et al. 2001). As organic compounds can also be subject to vertical relocation, the estimated ages of the sediments (similarly to the PTE-based estimates) are maximum ages and might be biased in terms of overestimation. To limit this, the detected compounds were restricted to the nonpolar forms, and thus to the greatest possible extent of immobile compounds.

As in Sect. “Discussion”, the younger reference date is 2014 AD, when the sampling was undertaken. As the older reference date, the years of the market introduction of these compounds were determined, including an additional 5 years to represent the likely delay in them entering the environment. Accordingly, the deepest occurrence of a particular substance in the cores provided the depth above which the sediment thickness could be converted into a mean annual sedimentation rate (see Table 5). The selected substance groups (PCNs, PCBs, and LABs) were introduced during different decades of the twentieth century. Figures 3, 4 and 5 thereby depict concentration values only for PCBs, since measured concentrations of PCNs and LABs were very low. PCNs were introduced c. 1910 AD (Falandyz 1998), PCBs

c. 1930 AD (Shiu and Mackay 1986), and LABs c. 1960 AD (Zeng and Yu 1996). Where one compound was detected within a sample, the upper boundary of the sample depth (i.e., 15 cm, 35 cm, 65 cm, 85 cm, or 95 cm) was chosen as the maximum depth of occurrence. This aimed to account for the large spacing of the geochemical bulk samples. Where a compound was detected, a possible presence in the sediment between the sampled layers cannot be discounted. Accordingly, the youngest compound group identified within a subsample indicated the maximum age and a corresponding minimum sedimentation rate. Therefore, it was possible to identify changes in sedimentation rates within a profile. In the case of core 1, LABs were detected up to 40 cm depth and PCBs up to 70 cm. This gave a sedimentation rate of at least 1.3 cm a^{-1} for 0–65 cm depths and 0.7 cm a^{-1} for 65–85 cm depths (see Table 5). As LABs were identified in the lowermost samples in core 2 and core 3, the estimated sedimentation rates were both 1.8 cm a^{-1} .

Estimation of sedimentation rates via numerical modeling

Using the Delft3D-FLOW model, sedimentation rates were determined by cumulating the sedimentation for the transect on the left floodplain post-1800 AD and dividing this by the modeled time. Modeling of historical river characteristics requires reasonable input and boundary conditions. Here, historical river bank heights and sedimentation rates—determined using the inorganic and organic geochemistry analysis results—were used to calibrate the historical model and to analyze floodplain deposition and fluvial morphodynamics. Based on the modeling, the mean sedimentation rate over the last 200 years was 0.7 cm a^{-1} across the sampling transect. Individually, the modeled sedimentation rates decreased from 0.8 cm a^{-1} for core 1 and core 2 to 0.6 cm a^{-1} for core 3.

As the following examples show, Delft3D is a commonly used software for modeling river and as estuarine hydro- and morphodynamics. For example, Frings et al. (2011) analyzed the effects of selective transport processes, overbank deposition, and channel migration on downstream fining in sandy lowland rivers. Kleinhans et al. (2018) compared the isolated and combined effects of mud and vegetation on river planform and morphodynamics in intermediate-sized valley rivers, and focused on the century-scale simulation of flow, sediment transport, and morphology coupled with riparian vegetation. Pu (2016) also used the Delft3D hydrodynamic module to analyze thermal changes in marine areas surrounding Singapore Island associated with different wave simulations.

Here, a the long-term numerical modeling approach was adopted, which is not comparable to other short-term hydro- and morphodynamic research. Local processes such as river

bank erosion are not included in the model. River bank erosion processes are often simulated in a single simplified numerical model or by separated numerical models, neither of which was applied here. Rinaldi et al. (2008) analyzed river bank erosion processes at one specific meander bend during one single flood event. The main purpose of their model was to parameterize fluvial erosion using outputs from detailed hydrodynamic simulations.

Model assumptions and schematizations are necessary and indispensable in nearly all numerical models, and these need to be evaluated to determine their effects on model quality (Warmink et al. 2011; Straatsma and Kleinhans 2018). Maaß and Schüttrumpf (2018) provide a general discussion of the model's quality to evaluate the effects of the quasi-steady hydrograph and the morphological scaling factor on the simulation results. They also assess the sensitivity of the model to sediment transport rates and sediment-size distribution.

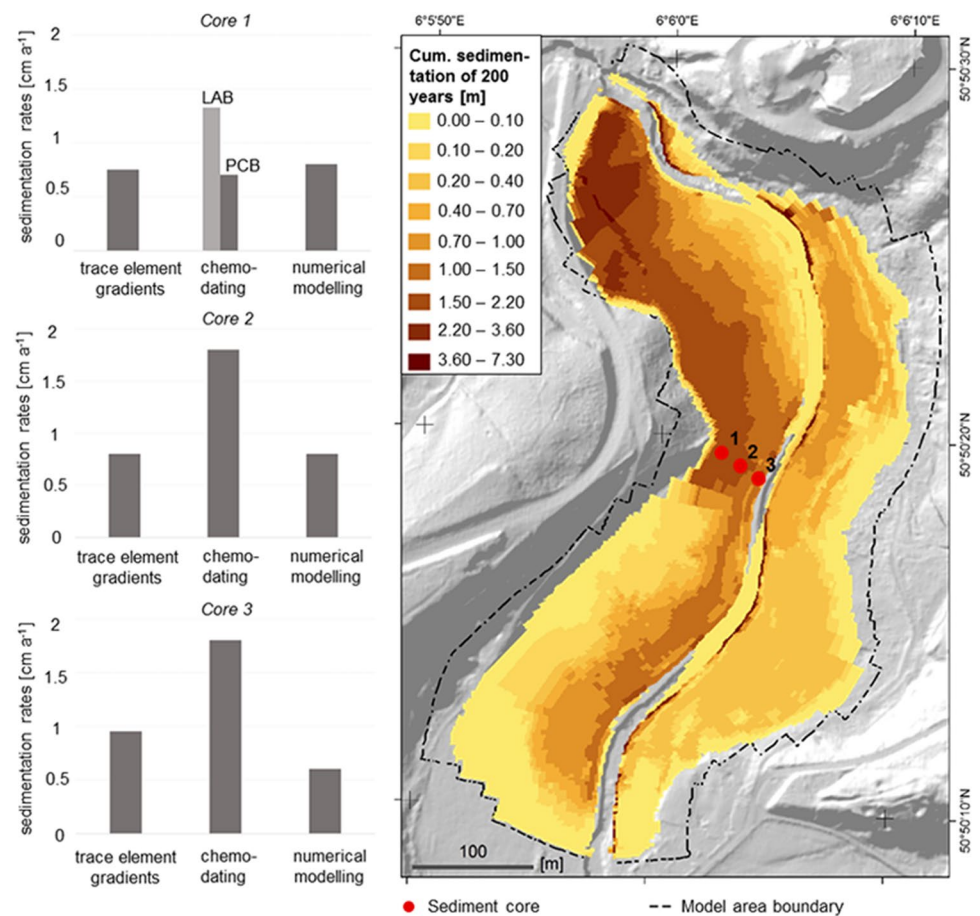
Combining the three approaches

The average sedimentation rates for each core based on approach 1 (trace elements) were 0.75 cm a^{-1} , 0.8 cm a^{-1} , and 0.9 cm a^{-1} , respectively, indicating an increase from the wall of the valley towards the natural levee and which corresponds to the geomorphological interpretation. The average rates for approach 2 ('chemodating' with organic xenobiotics) were 1.0 cm a^{-1} , 1.8 cm a^{-1} , and 1.8 cm a^{-1} , respectively. Again, these estimates support an increase in sedimentation rates towards the river channel. In contrast, approach 3 (numerical modeling) indicated a different spatial pattern with sedimentation rates decreasing from 0.8 cm a^{-1} at the wall of the valley to 0.6 cm a^{-1} at the natural levee.

The sedimentation rate values estimated using approach 1 and 3 were similar, whereas approaches 1 and 2 deviate by 0.05 cm a^{-1} to 0.65 cm a^{-1} (core 1), 0.9 cm a^{-1} (core 2), and 0.85 cm a^{-1} (core 3)—a difference of a factor of two near the river channel for core 2 and core 3. However, for the location of core 1, at the wall of the valley, the estimated sedimentation rates based on approach 1 and 2 were similar.

Overall, the transect analyzed in this study is typical of a natural levee channel with a floodplain sloping towards a backswamp approximately 0.5 m above the water table. The numerical model indicated higher sedimentation rates at the levee and lower sedimentation rates in the backswamp; this trend cannot be derived solely from a comparison of the three field cores. As the simulations assumed a cohesive sediment with a D_{50} grain size of $24.5 \mu\text{m}$, the sedimentation of coarse sediment was not included. Furthermore, numerical models are sensitive to their initial and boundary parameters; the effects of parameters such as the spatial resolution of the grid, the simplification of the inflow discharge to a quasi-steady hydrograph, and the application of

Fig. 7 Estimated mean sedimentation rates derived by three different approaches (left) and numerically modeled cumulative sedimentation over a 200-year period (right)



a morphological scaling factor. However, sensitivity analysis showed that these parameters did not significantly change the model results. Modeling of historical conditions does, in particular, involve uncertainties. Historical field data including topography, bathymetry, and sediment supply often do not exist and are difficult to measure directly. Here, the calibration of the numerical model was based on the results of the trace element and organic geochemistry analysis.

Sedimentation rates can successfully be determined by analyzing trace element gradients, organic xenobiotics, and numerical modeling in isolation; here each of these methods independently generated reasonable data that are comparable to other similar studies and locations (e.g., Leenaers 1989; Stam 2002: 0.4–2.7 cm a⁻¹ for the Geul River; and Maaß et al. 2018: 2 cm a⁻¹ for the Inde River). When compared, these approaches were mainly in good agreement (Fig. 7). However, for some locations the results based on the organic geochemistry data were up to two times higher than those obtained using the other approaches. Accordingly, the integration of multi-method data provided a more detailed understanding of the small river system studied here, as the application of a single approach would otherwise misrepresent the complexity of the system. To better understand river-floodplain systems in Central Europe with similar

catchment sizes and discharge regimes, and which are heavily impacted by human activities, a multi-proxy approach based on the integration of geomorphology, organic chemistry, and hydrology is recommended.

Conclusions

A multi-proxy approach was evaluated for studying the development of small meandering gravel-bed rivers with large floodplains, and estimated sedimentation rates for the last 200 years. Based on the interdisciplinary investigation, the following conclusions can be stated:

- Contaminant signals and different classes of anthropogenic impacts were successfully distinguished from the studied alluvial sediments. The impact classes reflected the historical development of anthropogenic activities since the pre-industrial era and enabled a qualitative assessment of the degree of pollution. In other catchments, local threshold values will vary depending on the geogenic background and the nature of anthropogenic activity and, therefore, assessments of these should be

based on analytical results of the area under investigation.

- Sedimentation rates were successfully derived by means of vertical gradient analysis of trace elements, the occurrence of organic contaminants, and numerical modelings. Each method generated reasonable results independently, but their comparison revealed general similarities—and some disparities—that helps create a more detailed understanding of such floodplain-river systems. Depending on the applied approach, the estimated mean sedimentation rates varied in a range 0.6–1.3 cm a⁻¹.
- The degree of recent and historical pollution of alluvial sediments and diachronic sedimentation rates varied explicitly over a small scale (across a 60-m transect and within 2-m cores), whereas less variability might have been initially expected.
- Investigations of floodplain pollution should not rely solely on bank profiles but must incorporate core drilling or similar field-sampling methods to capture the two-dimensional variability of geochemical signals, thus taking the architecture of alluvial sediments and changes in sedimentary facies into account.

The study site examined here is representative of Central European foothills and lowland rivers that have experienced a long history of anthropogenic pollution from industry, agriculture, and municipal waste water, and which have elevated concentrations of trace elements and organic xenobiotics as a result. In these contexts, a better understanding of the spatial variability of pollutants is important for river management and environmental planning. The proposed combination of multi-method approaches can be applied to other river systems with similar catchment sizes and topography. Through a combination of approaches, the assessment of anthropogenic impact, the estimation of sedimentation rates, and the overall understanding of fluvial morphodynamics can be improved. However, further research of low-order stream basins is necessary to link the evidence of small-scale spatial variability in the nature and extent of pollution to larger reaches in a supraregional context.

Acknowledgements Roy Frings is kindly acknowledged for his effort and advice in the development of the research project on which this publication is based. The authors thank Wolfgang Römer, Verena Esser, and two anonymous reviewers for valuable comments that strongly improved the manuscript. The cross-sectional profiles were kindly provided by Bezirksregierung Köln, Dezernat 54, Wasserwirtschaft.

Funding This work was supported by Deutsche Forschungsgemeinschaft (Grant numbers LE730/33-1, SCHW750/18-1, and FR3509/3-1).

Compliance with ethical standards

Conflict of interest The authors declare that they have no conflicts of interest.

References

- ABANDA (2013) Abfallanalysedatenbank ABANDA. Recklinghausen: Landesamt für Umwelt und Verbraucherschutz Nordrhein-Westfalen. <http://www.lanuv.nrw.de/abfall/bewertung/abanda.htm>. Accessed 26 Jan 2013
- Adánez Sanjuán P, Llamas Borrajo JF, Locutura Rupérez J, García Cortés A (2014) A geochemical study of overbank sediments in an urban area (Madrid, Spain). *Environ Geochem Health* 36:1129–1150. <https://doi.org/10.1007/s10653-014-9624-5>
- Bábek O, Faměra M, Hilscherová K et al (2011) Geochemical traces of flood layers in the fluvial sedimentary archive; implications for contamination history analyses. *Catena* 87:281–290. <https://doi.org/10.1016/j.catena.2011.06.014>
- Bell FG, Stacey TR, Genske DD (2000) Mining subsidence and its effect on the environment: some differing examples. *Environ Geol* 40:135–152. <https://doi.org/10.1007/s002540000140>
- Berger M, Löffler D, Ternes T et al (2016) The effect of distribution processes on the isomeric composition of hexachlorocyclohexane in a contaminated riverine system. *Int J Environ Sci Technol* 13:995–1008. <https://doi.org/10.1007/s13762-016-0940-4>
- Bezirksregierung Köln (2017) Historische Karten NRW. http://www.bezreg-koeln.nrw.de/brk_internet/geobasis/sonstige/historische_karten/index.html. Accessed 1 Apr 2017
- Birch GF, Robertson E, Taylor SE, McConchie DM (2000) The use of sediments to detect human impact on the fluvial system. *Environ Geol* 39:1015–1028. <https://doi.org/10.1007/s002549900075>
- Bruckner C (1967) Zur Wirtschaftsgeschichte des Regierungsbezirks Aachen. Rheinisch-Westfälisches Wirtschaftsarchiv zu Köln, Köln
- Buchty-Lemke M (2018) Untersuchungen zu anthropogenen Einflüssen auf die fluviale Morphodynamik und die Verteilung erhöhter Spurenelementgehalte in kleinen Flusseinzugsgebieten—Das Beispiel der Wurm, Flussgebietseinheit Maas. Dissertation, RWTH Aachen University, Aachen
- Buchty-Lemke M, Lehmkuhl F (2018) Impact of abandoned water mills on Central European foothills to lowland rivers: a reach scale example from the Wurm River, Germany. *Geogr Ann Ser Phys Geogr* 0:1–19. <https://doi.org/10.1080/04353676.2018.1425621>
- Callender E (2014) 11.3—heavy metals in the environment—historical trends. In: Holland HD, Turekian KK (eds) *Treatise on geochemistry*, 2nd edn. Elsevier, Oxford, pp 59–89
- Ciszewski D, Grygar TM (2016) A review of flood-related storage and remobilization of heavy metal pollutants in river systems. *Water Air Soil Pollut* 227:239. <https://doi.org/10.1007/s11270-016-2934-8>
- Curdes G (1999) Die Entwicklung des Aachener Stadtraumes—Der Einfluss von Leitbildern und Innovationen auf die Form der Stadt. Dortmund: Vertrieb für Bau- und Planungsliteratur, Dortmund
- Dahmen DJ (1925) Das Aachener Tuchgewerbe bis zum Ende des 19. Jahrhunderts—Ein Beitrag zur Wirtschaftsgeschichte der Stadt Aachen. Aachen: Aachener Verlags und Druckerei-Gesellschaft
- Deltares (2016) Delft Flow: simulation of multi-dimensional hydrodynamic flows and transport phenomena, including sediments. User Manual, 3D/2D modelling suite for integral water solutions. https://oss.deltares.nl/documents/183920/185723/Delft_3D-FLOW_User_Manual.pdf. Accessed 12 July 2019
- de Miguel E, Llamas JF, Chacón E et al (1997) Origin and patterns of distribution of trace elements in street dust: unleaded petrol and urban lead. *Atmos Environ* 31:2733–2740. [https://doi.org/10.1016/S1352-2310\(97\)00101-5](https://doi.org/10.1016/S1352-2310(97)00101-5)
- De Vos W, Ebbing J, Hindel R, Schalich J, Swennen R, Van Keer I (1996) Geochemical mapping based on overbank sediments

- in the heavily industrialised border area of Belgium, Germany and the Netherlands. *J Geochem Explor* 56:91–104. [https://doi.org/10.1016/0375-6742\(96\)00009-X](https://doi.org/10.1016/0375-6742(96)00009-X)
- Demetriades A, Pirc S, De Vos WD et al (2006) Distribution of elements in floodplain sediment. In: De Vos W, Travainin T, Reeder S (eds) *Geochemical atlas of Europe. Part. Geological survey of Finland, Espoo*, pp 41–44
- Dhivert E, Grosbois C, Rodrigues S, Desmet M (2015) Influence of fluvial environments on sediment archiving processes and temporal pollutant dynamics (Upper Loire River, France). *Sci Total Environ* 505:121–136. <https://doi.org/10.1016/j.scitotenv.2014.09.082>
- Dobler L (2000) Schwermetalltieftengradienten in Auensedimenten der Selke als Ausdruck der historischen Montanwirtschaft im Ostharz. In: Wippermann T (ed) *Bergbau und Umwelt: langfristige geochemische Einflüsse*; 39 Tabellen. Springer, Berlin, pp 67–85
- Eganhouse RP (1986) Long-chain alkylbenzenes: their analytical chemistry, environmental occurrence and fate. *Int J Environ Anal Chem* 26:241–263. <https://doi.org/10.1080/03067318608077118>
- Elznicová J, Grygar TM, Popelka J, Sikora M, Novák P, Hošek M (2019) Threat of pollution hotspots reworking in river systems: case study of the Ploučnice River (Czech Republic). *ISPRS Int J Geo-Inf* 1:2. <https://doi.org/10.3390/ijgi8010037>
- Eschweiler O, van Eyll K (eds) (2000) *Wirtschaftsgeschichte der Region Aachen: vom Ende des Zweiten Weltkriegs bis zur Gegenwart. Rheinisch-Westfälisches Wirtschaftsarchiv zu Köln, Köln*
- Famera M, Babek O, Matys Grygar T, Novakova T (2013) Distribution of heavy-metal contamination in regulated river-channel deposits: a magnetic susceptibility and grain-size approach; River morava, Czech republic. *Water Air Soil Pollut*. <https://doi.org/10.1007/s11270-013-1525-1>
- Falandysz J (1998) Polychlorinated naphthalenes: an environmental update. *Environ Pollut* 101:77–90. [https://doi.org/10.1016/S0269-7491\(98\)00023-2](https://doi.org/10.1016/S0269-7491(98)00023-2)
- Fikarová J, Kenecká S, Elznicová J, Faměra M, Lelková T, Matkovič J, Matys Grygar T (2018) Spatial distribution of organic pollutants (PAHs and polar pesticides) in the floodplain of the Ohře (Eger) River, Czech Republic. *J Soils Sediments* 18:259–275. <https://doi.org/10.1007/s11368-017-1807-0>
- Fischer R (2000) Entwicklung der Gewässergüte in der Wurm. In: *Landesumweltamt NRW (Hrsg) Gewässergütebericht 2000—30 Jahre Biologische Gewässerüberwachung in Nordrhein-Westfalen*. Essen: Landesumweltamt NRW, pp 215–224
- Förstner U (2004) Sediment dynamics and pollutant mobility in rivers: an interdisciplinary approach. *Lakes Reserv Res Manag* 9:25–40. <https://doi.org/10.1111/j.1440-1770.2004.00231.x>
- Frings RM, Ottevanger W, Sloff K (2011) Downstream fining processes in sandy lowland rivers. *J Hydraul Res* 49:178–193. <https://doi.org/10.1080/00221686.2011.561000>
- Frings RM, Gehres N, Promny M et al (2014) Today's sediment budget of the Rhine River channel, focusing on the Upper Rhine Graben and Rhenish Massif. *Geomorphology* 204:573–587. <https://doi.org/10.1016/j.geomorph.2013.08.035>
- Germershausen L (2013) Auswirkungen der Landnutzung auf den Schwermetall- und Nährstoffhaushalt in der Innersteaue zwischen Langelsheim und Ruthe. *Inst. für Geographie, Hildesheim*
- Gevao B, Harner T, Jones KC (2000) Sedimentary record of polychlorinated naphthalene concentrations and deposition fluxes in a dated lake core. *Environ Sci Technol* 34:33–38. <https://doi.org/10.1021/es990663k>
- Gocht T, Moldenhauer K-M, Püttmann W (2001) Historical record of polycyclic aromatic hydrocarbons (PAH) and heavy metals in floodplain sediments from the Rhine River (Hessisches Ried, Germany). *Appl Geochem* 16:1707–1721. [https://doi.org/10.1016/S0883-2927\(01\)00063-4](https://doi.org/10.1016/S0883-2927(01)00063-4)
- Grigoriadou A, Schwarzbauer J (2011) Non-target screening of organic contaminants in sediments from the industrial coastal area of Kavala City (NE Greece). *Water Air Soil Pollut* 214:623–643. <https://doi.org/10.1007/s11270-010-0451-8>
- Grygar TM, Sedláček J, Bábek O et al (2012) Regional contamination of Moravia (South-Eastern Czech Republic): temporal shift of Pb and Zn loading in fluvial sediments. *Water Air Soil Pollut* 223:739–753. <https://doi.org/10.1007/s11270-011-0898-2>
- Grygar TM, Elznicová J, Tůmová Š, Faměra M, Balogh M, Kiss T (2016) Floodplain architecture of an actively meandering river (the Ploučnice River, the Czech Republic) as revealed by the distribution of pollution and electrical resistivity tomography. *Geomorphology* 254:41–56. <https://doi.org/10.1016/j.geomorph.2015.11.012>
- Hagemann L, Buchty-Lemke M, Lehmkühl F, Alzer J, Kümmerle EA, Schwarzbauer J (2018) Exhaustive screening of long-term pollutants in riverbank sediments of the Wurm River, Germany. *Water Air Soil Pollut* 229:197. <https://doi.org/10.1007/s11270-018-3843-9>
- Hasse S (2000) *Giesserei Lexikon*. Fachverlag Schiele & Schön, Berlin
- Havlik D (2001) Das Wetter in Aachen im 20. Jahrhundert—Eine Bilanz. In: *Informationen und Materialien zur Geographie der Euregio Maas-Rhein*. Aachen, pp 62–73
- Heim S, Schwarzbauer J, Kronimus A et al (2004) Geochronology of anthropogenic pollutants in riparian wetland sediments of the Lippe River (Germany). *Org Geochem* 35:1409–1425. <https://doi.org/10.1016/j.orggeochem.2004.03.008>
- Heim S, Ricking M, Schwarzbauer J, Littke R (2005) Halogenated compounds in a dated sediment core of the Teltow canal, Berlin: time related sediment contamination. *Chemosphere* 61:1427–1438. <https://doi.org/10.1016/j.chemosphere.2005.04.113>
- Heim S, Hucke A, Schwarzbauer J, Littke R, Mangini A (2006) Geochronology of anthropogenic contaminants in dated sediment core of the Rhine River (Germany): emission sources and risk assessment. *Acta Hydrochim Hydrobiol* 34:34–52. <https://doi.org/10.1002/ahch.200500609>
- Heitfeld M, Mainz M, Schetelig K (2005) Post mining hazard assessment in North Rhine-Westphalia (Germany) at the example of the Aachen hard coal mining district. *Post-Mining* 2005, 16–17. Nancy, France. https://inis.iaea.org/collection/NCLCollectionStore/_Public/38/027/38027830.pdf?r=1&r=1. Accessed 12 July 2019
- Hillenbrand T, Toussaint D, Böhm E, et al (2005) Einträge von Kupfer, Zink und Blei in Gewässer und Böden. *Analyse der Emissionspfade und möglicher Emissionsminderungsmaßnahmen*; Forschungsbericht 20224220/02 UBA-FB 000824
- Hindel R, Schalich J, De Vos W et al (1996) Vertical distribution of elements in overbank sediment profiles from Belgium, Germany and The Netherlands. *J Geochem Explor* 56:105–122. [https://doi.org/10.1016/0375-6742\(96\)00010-6](https://doi.org/10.1016/0375-6742(96)00010-6)
- Hoffmann T, Thorndycraft VR, Brown AG et al (2010) Human impact on fluvial regimes and sediment flux during the Holocene: review and future research agenda. *Glob Planet Change* 72:87–98. <https://doi.org/10.1016/j.gloplacha.2010.04.008>
- Hoppmann A (2006) Integrierte Gewässerbewirtschaftung im Einzugsgebiet der Rur. In: Reineke T, Lehmkühl F, Blümel H (eds) *Grenzüberschreitendes integratives Gewässermanagement*. Academia Verlag, Sankt Augustin, p 254
- Hudson-Edwards KA, Macklin MG, Curtis CD, Vaughan DJ (1998) Chemical remobilization of contaminant metals within floodplain sediments in an incising river system: implications for dating and chemostratigraphy. *Earth Surf Process Landf* 23:671–684. [https://doi.org/10.1002/\(SICI\)1096-9837\(199808\)23:8%3c671:AID-ESP871%3e3.0.CO;2-R](https://doi.org/10.1002/(SICI)1096-9837(199808)23:8%3c671:AID-ESP871%3e3.0.CO;2-R)
- Hürkamp K, Raab T, Völkel J (2009a) Two and three-dimensional quantification of lead contamination in alluvial soils of a historic

- mining area using field portable X-ray fluorescence (FPXRF) analysis. *Geomorphology* 110:28–36. <https://doi.org/10.1016/j.geomorph.2008.12.021>
- Hürkamp K, Raab T, Völkel J (2009b) Lead pollution of floodplain soils in a historic mining area—age, distribution and binding forms. *Water Air Soil Pollut* 201:331–345. <https://doi.org/10.1007/s11270-008-9948-9>
- James CS (1985) Sediment transfer to overbank sections. *J Hydraul Res* 23:435–452. <https://doi.org/10.1080/00221688509499337>
- Kabata-Pendias A (2011) Trace elements in soils and plants, 4th edn. CRC Press, Boca Raton
- Käding M (2005) Rot(h)e Erden. In: Thomes P (ed) Rohstoffbasis und Absatzmarkt. Die Schwerindustrie des Großherzogtums Luxemburg und das Aachener Revier. Aachener Studien zur Wirtschafts- und Sozialgeschichte, Bd. 2. Aachen: Shaker Verlag, S. 13–20
- Kleinhans MG, de Vries B, Braat L, van Oorschot M (2018) Living landscapes: muddy and vegetated floodplain effects on fluvial pattern in an incised river. *Earth Surf Proc Land* 43:2948–2963. <https://doi.org/10.1002/esp.4437>
- Land NRW (ed) (2017) Datenlizenz Deutschland -Digitales Geländemodell Gitterweite 1 m—dl-de/by-2-0 (<http://www.govdata.de/dl-de/by-2-0>). <https://www.opengeodata.nrw.de/produkte/geobasis/dgm/dgm1/>. Accessed 1 Apr 2017
- Lenaers H (1989) The dispersal of metal mining wastes in the catchment of the river Geul (Belgium—The Netherlands). *Nederlandse Geografische Studies*. <http://dspace.library.uu.nl/handle/1874/13821>. Accessed 2 May 2018
- Legret M, Pagotto C (1999) Evaluation of pollutant loadings in the runoff waters from a major rural highway. *Sci Total Environ* 235:143–150. [https://doi.org/10.1016/S0048-9697\(99\)00207-7](https://doi.org/10.1016/S0048-9697(99)00207-7)
- Maaß A-L, Schüttrumpf H (2018) Long-term effects of mining-induced subsidence on the trapping efficiency of floodplains. *Anthropocene* 24:1–13. <https://doi.org/10.1016/j.ancene.2018.10.001>
- Maaß A-L, Schüttrumpf H (2019) Elevated floodplains and net channel incision as a result of the construction and removal of water mills. *Geografiska Annaler Ser A Phys Geogr* 101:157–176. <https://doi.org/10.1080/04353676.2019.1574209>
- Maaß A-L, Esser V, Frings RM, Lehmkuhl F, Schüttrumpf H (2018) A decade of fluvial morphodynamics: relocation and restoration of the Inde River (North-Rhine Westphalia, Germany). *Environ Sci Eur* 30:40. <https://doi.org/10.1186/s12302-018-0170-0>
- MacDonald DD, Ingersoll CG, Berger TA (2000) Development and evaluation of consensus-based sediment quality guidelines for freshwater ecosystems. *Arch Environ Contam Toxicol* 39:20–31. <https://doi.org/10.1007/s002440010075>
- Malmon DV, Dunne T, Reneau SL (2002) Predicting the fate of sediment and pollutants in River Floodplains. *Environ Sci Technol* 36:2026–2032. <https://doi.org/10.1021/es010509+>
- Malz F (1972) Über die Behandlung von Abwässern des Steinkohlenbergbaus. *Pure Appl Chem* 29:333–344. <https://doi.org/10.1351/pac197229010333>
- Martin CW (2015) Trace metal storage in recent floodplain sediments along the Dill River, central Germany. *Geomorphology* 235:52–62. <https://doi.org/10.1016/j.geomorph.2015.01.032>
- Meyer (1908) Meyer's Großes Konversations-Lexikon, Band 12. Leipzig, Wien: Bibliographisches Institut. <http://www.zeno.org/Meyers-1905/A/Leuchtgas>abger>. Accessed 2 Apr 2019
- Meyer L-H (1991) Kupfer- und Messingindustrie. In: Fehl G, Kaspari-Küffen D, Meyer L-H (eds) Mit Wasser und Dampf...: Zeitzeugen der frühen Industrialisierung im belgisch-deutschen Grenzraum. Meyer & Meyer, Aachen, pp 178–179
- Middelkoop H (2000) Heavy-metal pollution of the river Rhine and Meuse floodplains in the Netherlands. *Neth J Geosci* 79:411–427. <https://doi.org/10.1017/S0016774600021910>
- Middelkoop H (2002) Reconstructing floodplain sedimentation rates from heavy metal profiles by inverse modeling. *Hydrol Process* 16:47–64. <https://doi.org/10.1002/hyp.283>
- Ministerium für Klimaschutz, Umwelt, Landwirtschaft, Natur- und Verbraucherschutz des Landes Nordrhein-Westfalen (MKULNV NRW) (2009) Steckbrief der Planungseinheiten in den nordrhein-westfälischen Anteilen von Rhein, Weser, Ems und Maas. Düsseldorf
- Monaci F, Bargagli R (1997) Barium and other trace metals as indicators of vehicle emissions. *Water Air Soil Pollut* 100:89–98. <https://doi.org/10.1023/A:1018318427017>
- Mumbo J, Pandelova M, Mertes F et al (2016) The fingerprints of dioxin-like bromocarbazoles and chlorocarbazoles in selected forest soils in Germany. *Chemosphere* 162:64–72. <https://doi.org/10.1016/j.chemosphere.2016.07.056>
- Nagel DE, Buffington JM, Parkes SL, Wenger S, Goode JR (2014) A landscape scale valley confinement algorithm: delineating unconfined valley bottoms for geomorphic, aquatic, and riparian applications (no. RMRS-GTR-321). U.S. Department of Agriculture, Forest Service, Rocky Mountain Research Station, Ft. Collins, CO. <https://doi.org/10.2737/RMRS-GTR-321>
- Nicholas AP, Walling DE (1997) Investigating spatial patterns of medium-term overbank sedimentation on floodplains: a combined numerical modeling and radiocaesium-based approach. *Geomorphology* 19:133–150. [https://doi.org/10.1016/S0169-555X\(96\)00043-8](https://doi.org/10.1016/S0169-555X(96)00043-8)
- Nicholas AP, Walling DE (1998) Numerical modeling of floodplain hydraulics and suspended sediment transport and deposition. *Hydrol Process* 12:1339–1355. [https://doi.org/10.1002/\(SICI\)1099-1085\(19980630\)12:8%3c1339:AID-HYP618%3e3.0.CO;2-6](https://doi.org/10.1002/(SICI)1099-1085(19980630)12:8%3c1339:AID-HYP618%3e3.0.CO;2-6)
- Nichols G (2009) Sedimentology and stratigraphy, 2nd edn. Wiley-Blackwell, Chichester
- Nicholson FA, Smith SR, Alloway BJ et al (2003) An inventory of heavy metals inputs to agricultural soils in England and Wales. *Sci Total Environ* 311:205–219. [https://doi.org/10.1016/S0048-9697\(03\)00139-6](https://doi.org/10.1016/S0048-9697(03)00139-6)
- Nilson E (2006) Räumlich-strukturelle und zeitlich-dynamische Aspekte des Landnutzungswandels im Dreiländereck Belgien-Niederlande-Deutschland: eine Analyse mittels eines multitemporalen, multifaktoriellen und grenzübergreifenden Geographischen Informationssystems. Dissertation, RWTH Aachen University
- Nordrhein-Westfalen L (2005) Gewässerstrukturgüte in Nordrhein-Westfalen—Bericht 2005. Ministerium für Umwelt, Naturschutz, Landwirtschaft und Verbraucherschutz des Landes Nordrhein-Westfalen, Essen
- Notebaert B, Piégay H (2013) Multi-scale factors controlling the pattern of floodplain width at a network scale: the case of the Rhône basin, France. In: *Geomorphology, the field tradition in geomorphology 43rd annual Binghamton geomorphology symposium*, held 21–23 September 2012 in Jackson, Wyoming USA 200, pp 155–171. <https://doi.org/10.1016/j.geomorph.2013.03.014>
- Novakova T, Matys Grygar T, Babek O, Famera M, Mihaljevic M, Strnad L (2013) Human impact on fluvial sediments: how to distinguish regional and local sources of heavy metals contamination. Presented at the E3S Web of Conferences. <https://doi.org/10.1051/e3sconf/20130116008>
- Owens PN, Batalla RJ, Collins AJ et al (2005) Fine-grained sediment in river systems: environmental significance and management issues. *River Res Appl* 21:693–717. <https://doi.org/10.1002/rra.878>
- Paul J (1994) Grenzen der Belastbarkeit—Die Flüsse Rur (Roer) und Inde im Industriezeitalter. Verlag der Joseph-Kuhl-Gesellschaft, Jülich

- Perry C, Taylor K (2009) Environmental sedimentology: introduction. In: Perry C, Taylor K (eds) Environmental sedimentology. Blackwell, Malden, Oxford, Victoria, pp 1–31
- Phillips JM, Russell MA, Walling DE (2000) Time-integrated sampling of fluvial suspended sediment: a simple methodology for small catchments. *Hydrol Process* 14:2589–2602. [https://doi.org/10.1002/1099-1085\(20001015\)14:14%3c2589:AID-HYP94%3e3.0.CO;2-D](https://doi.org/10.1002/1099-1085(20001015)14:14%3c2589:AID-HYP94%3e3.0.CO;2-D)
- Pizzuto JE (1987) Sediment diffusion during overbank flows. *Sedimentology* 34:301–317. <https://doi.org/10.1111/j.1365-3091.1987.tb00779.x>
- Pu JH (2016) Conceptual hydrodynamic-thermal mapping modeling for coral reefs at south Singapore sea. *Appl Ocean Res* 55:59–65. <https://doi.org/10.1016/j.apor.2015.11.011>
- Pu JH, Lim SY (2014) Efficient numerical computation and experimental study of temporally long equilibrium scour development around abutment. *Environ Fluid Mech* 14:69–86. <https://doi.org/10.1007/s10652-013-9286-3>
- Rahbani M (2015) A comparison between the suspended sediment concentrations derived from DELFT3D model and collected using transmissometer—a case study in tidally dominated area of Dithmarschen Bight. *Oceanologia* 57:44–49. <https://doi.org/10.1016/j.oceano.2014.06.002>
- Reischl A, Joneck M, Dumler-Grادل R (2005) Chlorcarbazole in Böden. *Umweltwissenschaften Schadst-Forsch* 17:197. <https://doi.org/10.1065/uwsf2005.10.105>
- Rinaldi M, Mengoni B, Luppi L, Darby SE, Mosselman E (2008) Numerical simulation of hydrodynamics and bank erosion in a river bend. *Water Resour Res*. <https://doi.org/10.1029/2008WR007008>
- Salminen R, Batista MJ, Bidovec M et al (2005) Geochemical Atlas of Europe, part 1, background information, methodology and maps. Geological Survey of Finland
- Schmidt-Wygash CM (2011) Neue Untersuchungen zu holozänen Genese des Unterlaufs der Inde-Chronostratigraphische Differenzierung der Auenlehme unter besonderer Berücksichtigung der Montangeschichte der Voreifel. Dissertation, RWTH Aachen
- Schulte P, Lehmkuhl F, Steininger F et al (2016) Influence of HCl pretreatment and organo-mineral complexes on laser diffraction measurement of loess–paleosol-sequences. *CATENA* 137:392–405. <https://doi.org/10.1016/j.catena.2015.10.015>
- Schulze T, Ricking M (2005) Entwicklung einer Verfahrensrichtlinie “Sedimente und Schwebstoffe”. Freie Universität Berlin, Berlin
- Schwarzbauer J, Littke R, Weigelt V (2000) Identification of specific organic contaminants for estimating the contribution of the Elbe river to the pollution of the German Bight. *Org Geochem* 31:1713–1731. [https://doi.org/10.1016/S0146-6380\(00\)00076-0](https://doi.org/10.1016/S0146-6380(00)00076-0)
- Shiu WY, Mackay D (1986) A critical review of aqueous solubilities, vapor pressures, Henry’s law constants, and octanol-water partition coefficients of the polychlorinated biphenyls. *J Phys Chem Ref Data* 15:911–929. <https://doi.org/10.1063/1.555755>
- Stam MH (2002) Effects of land-use and precipitation changes on floodplain sedimentation in the nineteenth and twentieth centuries (Geul River, The Netherlands). In: Peterrtini I, Baker VR, Garzón G (eds) Flood and megaflood processes and deposits. Blackwell Publishing Ltd., Hoboken, pp 251–267
- Stelzer FH (2000) Die Steinkohlenaufbereitung und-verarbeitung auf den Zechen im Aachener Revier von den Anfängen bis zu den Zechenstilllegungen im historischen Kontext. In: Martens PN (Hrsg) Aachener Beiträge zur Rohstofftechnik und -wirtschaft Band 29. Verlag Mainz, Aachen
- Stock F, Knipping M, Pint A et al (2016) Human impact on Holocene sediment dynamics in the Eastern Mediterranean—the example of the Roman harbour of Ephesus: multi-proxy analyses of sediments of the Roman harbour of Ephesus. *Earth Surf Process Landf* 41:980–996. <https://doi.org/10.1002/esp.3914>
- Straatsma MW, Kleinhans MG (2018) Flood hazard reduction from automatically applied landscaping measures in RiverScape, a Python package coupled to a two-dimensional flow model. *Environ Model Softw* 101:102–116. <https://doi.org/10.1016/j.envsoft.2017.12.010>
- Swennen R, Van der Sluys J (2002) Anthropogenic impact on sediment composition and geochemistry in vertical overbank profiles of river alluvium from Belgium and Luxembourg. *J Geochem Explor* 75:93–105. [https://doi.org/10.1016/S0375-6742\(02\)00199-1](https://doi.org/10.1016/S0375-6742(02)00199-1)
- Swennen R, Keer IV, Vos WD (1994) Heavy metal contamination in overbank sediments of the Geul river (East Belgium): its relation to former Pb–Zn mining activities. *Environ Geol* 24:12–21. <https://doi.org/10.1007/BF00768072>
- Törnqvist TE, Bridge JS (2002) Spatial variation of overbank aggradation rate and its influence on avulsion frequency. *Sedimentology* 49:891–905. <https://doi.org/10.1046/j.1365-3091.2002.00478.x>
- Umweltbundesamt (2001) Abtrag von Kupfer und Zink von Dächern, Dachrinnen und Fallrohren durch Niederschläge. <https://www.umweltbundesamt.de/publikationen/abtrag-von-kupfer-zink-von-daechern-dachrinnen>. Accessed 13 May 2016
- Vogt H (1998) Niederrheinischer Wassermühlenführer. Krefeld
- von Coels L (1991) Zum gewerblich-industriellen Zustand von Aachen im Jahre 1836. In: Fehl G, Kaspari-Küffen D, Meyer L-H (eds) Mit Wasser und Dampf...: Zeitzeugen der frühen Industrialisierung im belgisch-deutschen Grenzraum. Meyer & Meyer, Aachen, p 163
- Walling D, Owens P, Carter J et al (2003) Storage of sediment-associated nutrients and contaminants in river channel and floodplain systems. *Appl Geochem* 18:195–220. [https://doi.org/10.1016/S0883-2927\(02\)00121-X](https://doi.org/10.1016/S0883-2927(02)00121-X)
- Warmink JJ, Van der Klis H, Booij MJ, Hulscher SJMH (2011) Identification and quantification of uncertainties in a hydrodynamic river model using expert opinions. *Water Resour Manag* 25:601–622. <https://doi.org/10.1007/s11269-010-9716-7>
- Weber U (1991) Einfluss der Urbanisierung auf den Wasserhaushalt im Raum Aachen. Geographisches Institut der RWTH Aachen im Selbstverlag, Aachen
- Wessels M, Lenhard A, Giovanoli F, Bollhöfer A (1995) High resolution time series of lead and zinc in sediments of Lake Constance. *Aquat Sci Res Boundaries* 57:291–304. <https://doi.org/10.1007/BF00878394>
- Witter B, Winkler M, Friese K (2004) Depth distribution of chlorinated and polycyclic aromatic hydrocarbons in floodplain soils of the River Elbe. *Acta Hydrochim Hydrobiol* 31:411–422
- Wrede V, Zeller M (1988) Geologie der Aachener Steinkohlelagerstätten. Krefeld
- Zeng EY, Yu CC (1996) Measurements of linear alkylbenzenes by GC/MS with interference from tetrapropylene-based alkylbenzenes: calculation of quantitation errors using a two-component model. *Environ Sci Technol* 30:322–328. <https://doi.org/10.1021/es9504045>

Publisher’s Note Springer Nature remains neutral with regard to jurisdictional claims in published maps and institutional affiliations.